Quantum Hall Response to Time-Dependent Strain Gradients in Graphene

Eran Sela,[1] Yakov Bloch,[1] Felix von Oppen,[2] and Moshe Ben Shalom[1]
[1]Raymond and Beverly Sackler School of Physics and Astronomy, Tel-Aviv University, IL-69978 Tel Aviv, Israel
[2]Dahlem Center for Complex Quantum Systems and Fachbereich Physik, Freie Universität Berlin, 14195 Berlin, Germany

(Received 26 September 2019; published 16 January 2020)

Mechanical deformations of graphene induce a term in the Dirac Hamiltonian that is reminiscent of an electromagnetic vector potential. Strain gradients along particular lattice directions induce local pseudomagnetic fields and substantial energy gaps as indeed observed experimentally. Expanding this analogy, we propose to complement the pseudomagnetic field by a pseudoelectric field, generated by a time-dependent oscillating stress applied to a graphene ribbon. The joint Hall-like response to these crossed fields results in a strain-induced charge current along the ribbon. We analyze in detail a particular experimental implementation in the (pseudo)quantum Hall regime with weak intervalley scattering. This allows us to predict an (approximately) quantized Hall current that is unaffected by screening due to diffusion currents.

DOI: 10.1103/PhysRevLett.124.026602

Graphene offers a fertile ground to explore the rich physics of crystalline Dirac materials. A simple tight binding Hamiltonian with a constant hopping amplitude t between carbon atoms gives a fair band structure description of many graphene-based systems. Famous examples include single layer graphene with its linearly dispersing (massless) Dirac fermions [1,2], electrically biased bilayers with a displacement-field-induced band gap [3,4], or twisted layers with (almost) nondispersing (flat) bands and externally tunable electron correlations [5,6]. Graphene is also outstanding in its mechanical stability. The unit cell can stretch by more than 20% without breaking [7], thus allowing for significant tuning of t by applying external stress [8–10]. Combining these unique electronic and mechanical resources is highly appealing, and promises novel "straintronic" phenomena.

One challenge is to open band gaps by straining the monoatomic hexagonal lattice. The two Dirac points appearing near the K and K' points are protected against perturbations that keep inversion and time reversal symmetries intact, as is the case for uniform (possibly anisotropic) strain. Anisotropic strain replaces the single parameter t by three hopping amplitudes t_1, t_2, and t_3 [see Fig. 1(a)] and shifts the Dirac points in reciprocal space. Interestingly, the difference between the three amplitudes translates into a fictitious vector potential $\vec{A}$, appearing in the Dirac Hamiltonian [11], $H = v_F\vec{\sigma}\cdot(-i\hbar\vec{\nabla} \mp e\vec{A})$, with $eA_x = \frac{1}{2}(\hbar/at)(t_2 + t_3 - 2t_1)$ and $eA_y = (\sqrt{3}/2)(\hbar/at)(t_3 - t_2)$ (with $v_F = 10^6$ ms^{-1} as the Fermi velocity, $a = 1.4$ Å as the lattice spacing, and $t = 2.5$ eV). The strain-induced term $\vec{A}(\vec{r}, t)$, acts within each valley as an external electromagnetic vector potential. However, in order to preserve time reversal, this "pseudovector" potential acquires opposite signs in the two valleys. It can be expressed in terms of the strain tensor components ϵ_{ij} [11–13],

$$\vec{A} = \frac{\beta t}{e v_F}\begin{pmatrix} \epsilon_{xx} - \epsilon_{yy} \\ -2\epsilon_{xy} \end{pmatrix}, \tag{1}$$

with $\beta = -(d\log t/d\log a) \cong 2.5$. For carriers in a specific valley, the pseudovector potential $\vec{A}(\vec{r}, t)$ implies electric

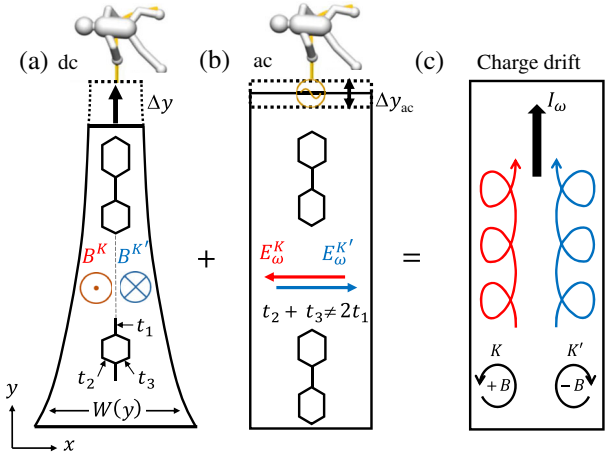

FIG. 1. (a) Graphene ribbon oriented along the armchair direction, with a uniaxial stretch generating a larger deformation at its narrow (top) end. The resulting strain gradient is designed via the shape function $W(y)$ to create a uniform pseudomagnetic field $\vec{B}$ (Ref. [22]). (b) A time varying (oscillating) stress component generates an additional pseudoelectric field $\vec{E}$. The orientations of both $\vec{B}$ and $\vec{E}$ are opposite for electrons in the K and K' valleys. (c) Illustration of the valley symmetric drift dynamics considering half an oscillating period so that $\vec{E}$ has a fixed sign.

 © 2020 American Physical Society

and magnetic fields. The former, $\vec{E} = -(d\vec{A}/dt)$, is induced by time-dependent strains, while the latter, $\vec{B} = (\vec{\nabla} \times \vec{A})_z \hat{z}$, requires specific strain gradients [13–17]. Experimentally, scanning tunneling spectroscopy [18,19] on triangularly strained graphene found tunneling resonances with a Landau-level-like spacing that indicated remarkably large pseudomagnetic fields $\vec{B}$ exceeding 300 T. Recent angle-resolved photoemission spectra [20] on multiple triangular islands of graphene further confirm the pseudo-Landau level (PLL) picture of flat bands separated by over ~100 meV. The large energy gaps exceed room temperature and promise fascinating correlation physics, as well as practical technological opportunities. Detecting the pseudoelectric $\vec{E}$ fields, on the other hand, remains challenging [21]. Unavoidable lattice deformations also induce a scalar potential $\phi(r,t) \propto \epsilon_{xx}(r,t) + \epsilon_{yy}(r,t)$ due to compression or dilation of the unit cell. While $\phi(r,t)$ acts equally on both valleys, the pseudoelectric field switches signs between the valleys and generates valley rather than charge currents.

Here we propose a way to observe the pseudoelectric field through charge currents by combining time-dependent and spatially varying strains that introduce both pseudo-E and pseudo-B fields. The concept is similar to the Hall effect, where a transverse drift velocity $\vec{v}_d = [(\vec{B} \times \vec{E})/|B|^2]$ is generated in the presence of nonparallel fields. While the direction of each individual field is opposite for electrons from the two valleys, the Hall-like drift velocity involves both fields and points in the same direction for both valleys.

We demonstrate this general concept in a particular and experimentally feasible geometry of a graphene ribbon under uniaxial stress [22]. As sketched in Fig. 1(a), we set the stress and the lattice armchair direction along the ribbon, while the width of the ribbon W is narrowing toward its top end. The stress leads to $t_1 \neq t_2$, t_3 for this orientation, while the change in W induces strain gradients and thus a pseudo-B field. To generate a pseudo-E field in the transverse direction, we add a small ac stress component to the fixed dc strain, see Fig. 1(b). Together, the two intrinsic fields generate a drift motion along the ribbon for electrons from both valleys and thus an oscillating charge current $\vec{I}_\omega$, see Fig. 1(c). Classically, the current is given by $I_\omega = ne(|E_x|/|B|)W$, where n is the density measured from the Dirac point. Defining the filling factor $\nu = (hn/eB)$, this nonquantized current translates into $I_\omega = (e^2/h)\nu V_\omega$, where $V_\omega \sim EW$ is an ac pseudovoltage difference induced by the intrinsic pseudo-E field. While in principle detectable, we show that $\vec{I}_\omega$ is usually minute for ac strain frequencies smaller than ~ gigahertz due to fast and efficient screening by diffusing electrons. Our main prediction is that a sizable charge response can be observed when the pseudo-B field is sufficiently strong to cause the formation of PLLs. In this regime, the presence of energy gaps efficiently suppresses screening and a Hall-like $\vec{I}_\omega$ is expected for a wide range of frequencies, deformations, and doping levels, provided that intervalley scattering is weak. We suggest a particular device realization where these requirements can be achieved and compare the conventional quantum Hall (QH) response for static magnetic fields, both externally applied and strain induced, to the dynamic pseudo-QH response, which is the main prediction of this Letter.

System.—We envision a micrometer scale geometry as shown in Fig. 2(a). The ribbon is clamped at the top and bottom ends and pulled by metallic beams, which are also used to measure the charge transport response. We compute the mechanical response ϵ_{ij} by COMSOL finite element simulations, adjusting the external stretch to $\Delta y \approx 100$ nm to induce a maximum local strain of 20%. Naturally, variations in the ribbon's width $W(y)$ translate into gradients in ϵ_{yy} along the y direction [see Fig. 2(c)], and hence to a finite (dA_x/dy). More specifically, the shape function $W(y)$ is selected to optimize a constant gradient in ϵ_{yy} and hence a uniform pseudo-B field over a large section of the ribbon [22,23]. The color map in Fig. 2(b) shows $B = (\nabla \times A)_z$ and the strain tensor components. For the specific dimensions presented, we obtain a nearly constant $B \cong 3$ T over 0.5 μm at the center of the ribbon [see the black line in Fig. 2(c)].

The local pseudo-E field is generated by a small ac stress applied in the same direction. We envision a mechanical piezoelectric manipulator that can modulate the strain at a

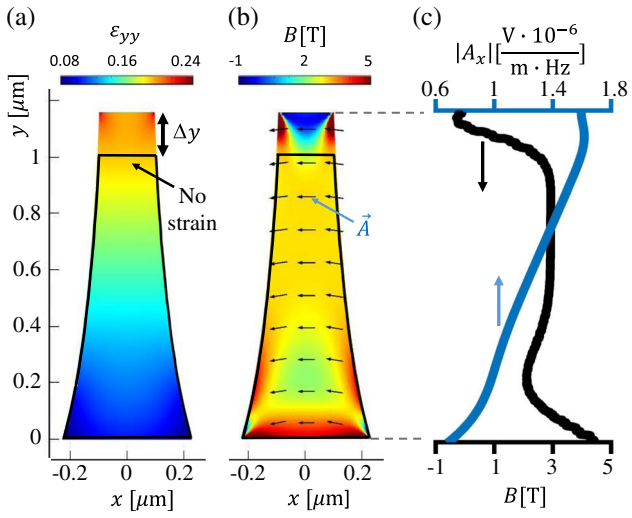

FIG. 2. (a) Strain tensor component $\epsilon_{yy}(x,y)$ calculated by COMSOL. We set the vertical stretch Δy to induce a maximum strain ϵ_{yy} of 20% (red). (b) Color plot of the calculated pseudomagnetic field $(\nabla \times \vec{A})_z$ and arrow plot of the pseudovector potential calculated from Eq. (1), determining the strength and direction of the pseudoelectric field for ac strain. (c) Profiles of B, showing a relatively uniform ≈3 T over a microscale region (blue), and of A_x, allowing one to extract the pseudovoltage of 0.1 mV (see text).

frequency of, say, $\omega = 10$ MHz, and assume a small oscillation amplitude such that the device elongates by $\pm\Delta y_{\rm ac}$, where $\Delta y_{\rm ac} \approx 10$ nm (leaving B approximately unchanged). The orientation of E and its magnitude (scaled by a factor $\Delta y_{\rm ac} \times \omega$) are determined by A and presented at several points in the ribbon by the arrows (size and orientation) in Fig. 2(b). The magnitude of A along the $x = 0$ line is plotted in Fig. 2(c). As shown, the arrows are pointing primarily in the x direction, indicating an ac pseudovoltage difference between the right and left sides of the ribbon. Upon integration, $V_\omega = \int dx E \sim WE$, we find a value $\sim$0.1 mV.

Using a simple elastic theory, one can also obtain analytic approximations of the two pseudofields [23], $E_x(y) = (\Delta y_{\rm ac}/L)\omega[1/(1 + f_r)][W(L)/W(y)][4(1 + \bar{\nu})\beta(t/ev_F)]$ and $B = (\Delta y/L)[(1 - f_r)/(1 + f_r)](1/L) \times 6(1 + \bar{\nu}) \times \beta(t/ev_F)$. In the latter, the three factors display the dependence on the ribbon's stretching deformation Δy, narrowing parameter $f_r = [W(L)/W(0)]$, and overall dimension L. In the last dimensionful factor, $\bar{\nu} \approx 0.17$ [22] is the Poisson ratio and $(t/ev_F) = 2.5\text{T}\mu\text{m}$. The field E_x depends directly on $\epsilon_{yy}(y)$ and thus increases along the narrowing ribbon as $1/W(y)$, see Fig. 2(c). Since the frequencies considered are low compared to all relevant electronic and elastic modes, we will treat the pseudo-E field as quasistatic.

Both the simulated and analytic results presented above show relatively large and uniform intrinsic fields over a micrometer size sample. Compared to the nanoscale systems considered to date, this leads to several advantages: finite size effects are minute, the magnetic length $l_B = \sqrt{(\hbar/eB)}$ is significantly smaller than the system size, and the cyclotron radius $r_c = (p_F/eB)$ can be tuned below the system's dimensions L, W by an external gate. Thus, the proposed system allows us to consider the QH regime with $\omega_c\tau \gg 1$ (with the cyclotron frequency $\omega_c = v_F/l_B$) generated by pure strain.

Quantum Hall regime: Static case.—Before considering ac strain and the associated pseudo-E field, we discuss transport in the integer QH regime, contrasting the case of an external magnetic field $B_{\rm ext}$ against an intrinsic pseudo-B field, as probed by a two-probe measurement.

Here, we focus on the clean case and argue that disorder just renders the QH physics more robust [26–28]. To visualize the LLs and PLLs for these two cases [Fig. 3(a)], consider a Corbino disk geometry (i.e., our geometry with a periodic and translation invariant y direction). We can then label states by their momenta k_y, which are related to x. For an external magnetic field $k_y = \text{const} + x/l_B^2$. In contrast, for a pseudo-B field, k_y and x are related differently for the two valleys, $k_y = \text{const}_\pm \pm x/l_B^2$. The current follows by summing over the contributions of all occupied states, $I = \sum_{k_y\text{occ}} I(k_y)$. Once the Fermi level lies in the bulk gap between LLs (or PLLs), each (P)LL contributes a quantized current [26,27]

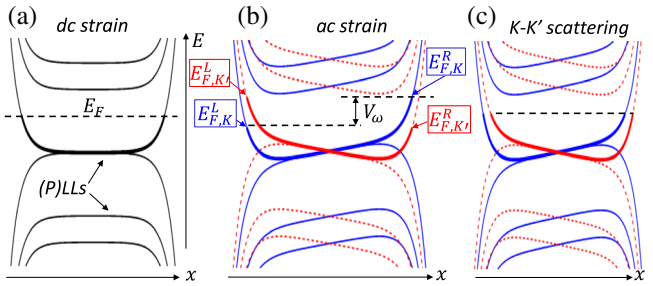

FIG. 3. (a) Plot of typical PLLs (or LLs) and edge states. (b) Tilting PLLs due to bulk pseudoelectric field caused by ac strain. A finite pseudovoltage difference V_ω between the edges is indicated. (c) Strong intervalley scattering causes equilibration within each edge.

$$I_{\rm LL} = \frac{e}{h}\int_{\rm occ} dk_y \frac{d\epsilon}{dk_y} = \frac{e^2}{h} V_{\rm ext} \tag{2}$$

in a two-terminal setup. Here, $V_{\rm ext}$ is the external voltage applied between the two terminals.

For an external magnetic field, the edge modes are chiral. The voltage at the source terminal feeds into one of the two edges, say the right edge, elevating its chemical potential for both valleys with respect to the opposite edge [29], i.e., $eV_{\rm ext} = E^R_{F,K} - E^L_{F,K} = E^R_{F,K'} - E^L_{F,K'}$. Summing over spin and valley, this leads to a sequence of quantized plateaus in the two-terminal conductance $(I/V_{\rm ext}) = (e^2/h)|\nu|$, where $\nu = \pm 2, \pm 6, \ldots$ (see the black dashed curve in Fig. 4). The current is quantized and protected by the large distance between the counterpropagating chiral edge modes.

The pseudo-B field, on the other hand, spatially superimposes counterpropagating edge states from the two valleys. Thus, the system is no longer protected against backscattering, and we expect a nonquantized two-terminal conductance [31,32]. The external voltage now imposes opposite interedge chemical potential differences in the two valleys, $eV_{\rm ext} = E^R_{F,K} - E^L_{F,K} = -(E^R_{F,K'} - E^L_{F,K'})$. Nevertheless, approximate quantization is expected if the disorder potential is smooth on the atomic scale and intervalley scattering is suppressed (see the blue curve in Fig. 4) [33,34]. This is possible, for example, by effectively introducing smooth edges [23].

A few comments on our assumptions for the formation of PLLs are in order. To obtain translation invariance along the y direction, we use the gauge $A_y = -Bx$ rather than $A_x = By$. Note that our synthetic gauge theory is actually not gauge invariant in the presence of generic intervalley coupling, since the two valleys transform differently. Gauge invariance applies only to each valley separately. Exploiting gauge invariance assumes that valley is a good quantum number. This requires negligible intervalley scattering both in the bulk and on the edges, as discussed above. Additionally, we comment that, while Fig. 3(a) shows flat bands, PLLs are not necessarily flat [35,36].

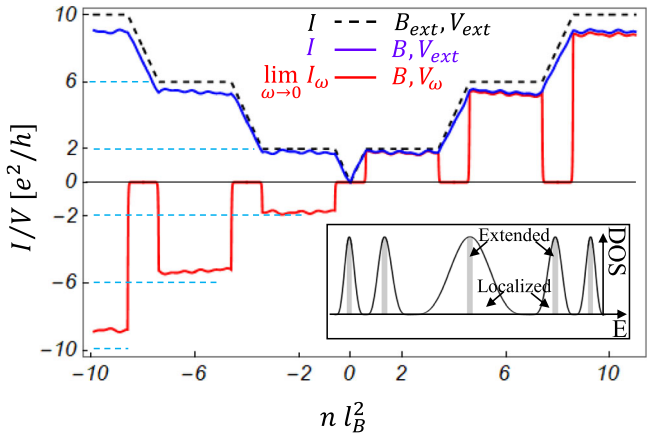

FIG. 4. Schematics of QH vs pseudo-QH response as a function of density near the Dirac point. (Black dashed line) Two-terminal quantized conductance for external magnetic field $B_{\rm ext}$ and a voltage $V_{\rm ext}$ applied through a chemical potential difference between the terminals. (Blue) Two-terminal conductance for a pseudomagnetic field B and voltage $V_{\rm ext}$; backscattering due to counterpropagating valleys leads to deviations from quantization. (Red) Alternating current response to simultaneous pseudo-B and pseudo-E fields generating an internal pseudovoltage difference V_ω. The current is approximately quantized at the plateaus, and strongly suppressed at the plateau transitions due to screening of the pseudo-E field [30]. (Inset) DOS consisting of extended states at the PLL energies surrounded by localized states.

Quantum Hall regime: Dynamic case.—Now, rather than considering a voltage difference between infinite reservoirs, we dynamically apply an intrinsic pseudo-E field, generating a potential difference $V_\omega = EW$ between the edges. This leads to oppositely tilting PLLs in the two valleys, as shown in Fig. 3(b). As long as a bulk gap remains open between the tilted PLLs, which requires $EW < \hbar\omega_c$, the current depends solely on the chemical potential difference between the edges. We have $eV_\omega = E^R_{F,K} - E^L_{F,K} = -(E^R_{F,K'} - E^L_{F,K'})$, so that Eq. (2) predicts approximately quantized plateaus for weak intervalley scattering (cf. the two-terminal case with pseudo-B field). Thus, in the gap-dominated regime, our ac pseudo-Hall effect is quantized $(I_\omega/V_\omega) = (e^2/h)\nu$ with $\nu = 4(N + 1/2)$, even at low frequencies. This alternating charge current in response to the pseudo-E field is our main result. The resulting plateaus are schematically displayed in Fig. 4 by the red curve. In the presence of intervalley scattering, we expect the edges to equilibrate, see Fig. 3(c). From the above estimate of a 0.1 mV pseudovoltage, we obtain $I_\omega \sim 8$ nA for filling factor $\nu = 2$.

We remark that in experiment one can rectify this ac I_ω into a dc. For example, adding an ac gate voltage, switching the electron density between two constant values ν_+ (ν_-) during the half period with pseudo-E field $E(t) > 0$ [$E(t) < 0$], one obtains an approximately quantized dc $(I_{\rm dc}/V_\omega) = (e^2/\pi h)(\nu_+ - \nu_-)$.

While the two-terminal conductance is necessarily positive, the pseudo-E response changes sign across the Dirac point (see the red curve in Fig. 4). This is a consequence of the sign change in the group velocity of the edge states upon going from electron to hole doping.

Another crucial difference between the external voltage $V_{\rm ext}$ between infinite reservoirs and the intrinsically generated transverse voltage V_ω is that the latter will be screened by electronic diffusion across the ribbon on timescales much faster than the ac frequency. This is reflected in the red curve in Fig. 4, where the current response drops to zero at QH transitions due to screening in these delocalized situations. The same effect of the pseudo-E field will occur for any gapless system, in particular, for small pseudo-B fields with $\omega_c\tau \ll 1$. We now discuss this screening at finite frequency within a semiclassical treatment.

Gapless (screened) regime.—The interplay of a dissipative conductivity σ with the edges of the sample and the resulting valley polarization can be described via the transport equation

$$\vec{j}_\pm = \pm\sigma\vec{E}_\omega - D\vec{\nabla}n_\pm \mp (\omega_c\tau)\vec{j}_\pm \times \hat{z}, \tag{3}$$

for the current densities $\vec{j}_\pm(x, y)$ and charge densities $n_\pm(x, y)$ of the two valleys. The conductivity σ is related to the diffusion coefficient D via the Einstein relation. The last term in Eq. (3) is a Hall term. The edges of the sample imply the boundary condition $j_x(x = 0, y) = j_x(x = W, y) = 0$. We provide a closed form solution of this equation (combined with the continuity equation) in the Supplemental Material [23]. It can be written in terms of two dimensionless parameters. In addition to $\omega_c\tau$, the typical timescale for traversing the sample, $\tau_T = W^2/D$, introduces a second dimensionless parameter $\omega\tau_T$, which controls the reduction of the current due to screening by valley-dependent diffusion currents.

For $\omega\tau_T \gg 1$, screening is not effective. In this regime, the current takes the Drude form $(I_\omega/V_\omega) = \{[\sigma(\omega_c\tau)]/[1 + (\omega_c\tau)^2]\}$ for an infinite system and is in phase with the pseudo-E field. At low frequencies, we find [23] $(I_\omega/V_\omega) = (i/12)\sigma(\omega\tau_T)(\omega_c\tau)$, which is out of phase with the pseudo-E field. In the system in Fig. 1, with $\omega = 10$ MHz, we estimate $\omega\tau_T \approx 10^{-3}$, leading to a strong reduction of the current at the QH transitions. For $\omega_c\tau \approx 1$, we obtain $I \sim p$A. In principle, however, the effect can be observed even in a gapless regime, provided the frequency is sufficiently high, $\omega\tau_T \gtrsim 1$.

Conclusion.—We presented a novel mechanism to generate charge currents from space- and time-dependent strain fields in graphene, by combining crossed pseudo-B and pseudo-E fields. A related charge current response was found [37] by gapping out graphene by a mass corresponding to a sublattice potential (e.g., due to h-BN encapsulation), which plays the role of the time reversal invariant and tunable PLL gap in our case. The charge current response should be contrasted with previous theoretical works on transport in strained graphene, predicting valley-polarized

currents in the presence of external magnetic fields [31,38–42], including valley filters or switches [43–49], by combination with polarized light [50], parametric pumping [51,52], or even in equilibrium in a zigzag graphene ribbon [36].

The relatively simple and analytic gauge field treatment of a long-wavelength strain in graphene allowed us to analyze inversion symmetry breaking on macroscopic scales, design a tunable static strain-induced bulk gap, and use these to induce a dynamic charge current. We expect this general concept to extend to a wider set of systems and materials, including (3D) Weyl semimetals, which show similar synthetic gauge field effects [53–57]. The proposed effect also allows for measuring the edge contribution to intervalley scattering, to which it is highly sensitive even in the static case.

We thank Roman Mints for useful discussions. This research was supported by the Binational Science Foundation Grant No. 2016255 (E. S.), CRC 183 of the Deutsche Forschungsgemeinschaft (F. v. O.), the Israel Science Foundation Grant No. 1652/18, and the European Research Council (ERC) under the European Unions Horizon 2020 Research and Innovation Programme Grant No. 852925 (M. B. S.).

[1] P. R. Wallace, Phys. Rev. **71**, 622 (1947).
[2] K. S. Novoselov, A. K. Geim, S. Morozov, D. Jiang, M. Katsnelson, I. Grigorieva, S. Dubonos, and A. A. Firsov, Nature (London) **438**, 197 (2005).
[3] E. McCann and V. I. Falko, Phys. Rev. Lett. **96**, 086805 (2006).
[4] E. V. Castro, K. S. Novoselov, S. V. Morozov, N. M. R. Peres, J. M. B. Lopes dos Santos, J. Nilsson, F. Guinea, A. K. Geim, and A. H. Castro Neto, Phys. Rev. Lett. **99**, 216802 (2007).
[5] R. Bistritzer and A. H. MacDonald, Proc. Natl. Acad. Sci. U.S.A. **108**, 12233 (2011).
[6] Y. Cao, V. Fatemi, S. Fang, K. Watanabe, T. Taniguchi, E. Kaxiras, and P. Jarillo-Herrero, Nature (London) **556**, 43 (2018).
[7] C. Lee, X. Wei, J. W. Kysar, and J. Hone, Science **321**, 385 (2008).
[8] B. Amorim, A. Cortijo, F. De Juan, A. Grushin, F. Guinea, A. Gutiérrez-Rubio, H. Ochoa, V. Parente, R. Roldán, P. San-Jose *et al.*, Phys. Rep. **617**, 1 (2016).
[9] C. Si, Z. Sun, and F. Liu, Nanoscale **8**, 3207 (2016).
[10] D. Akinwande, C. J. Brennan, J. S. Bunch, P. Egberts, J. R. Felts, H. Gao, R. Huang, J.-S. Kim, T. Li, Y. Li *et al.*, Ext. Mech. Lett. **13**, 42 (2017).
[11] J. L. Manes, Phys. Rev. B **76**, 045430 (2007).
[12] H. Suzuura and T. Ando, Phys. Rev. B **65**, 235412 (2002).
[13] F. Guinea, M. Katsnelson, and A. Geim, Nat. Phys. **6**, 30 (2010).
[14] K.-I. Sasaki, Y. Kawazoe, and R. Saito, Prog. Theor. Phys. **113**, 463 (2005).
[15] F. Guinea, A. K. Geim, M. I. Katsnelson, and K. S. Novoselov, Phys. Rev. B **81**, 035408 (2010).
[16] M. A. Vozmediano, M. Katsnelson, and F. Guinea, Phys. Rep. **496**, 109 (2010).
[17] D. Zhai and N. Sandler, Mod. Phys. Lett. B **33**, 1930001 (2019).
[18] N. Levy, S. Burke, K. Meaker, M. Panlasigui, A. Zettl, F. Guinea, A. C. Neto, and M. Crommie, Science **329**, 544 (2010).
[19] Y. Jiang, J. Mao, J. Duan, X. Lai, K. Watanabe, T. Taniguchi, and E. Y. Andrei, Nano Lett. **17**, 2839 (2017).
[20] P. Nigge, A. Qu, É. Lantagne-Hurtubise, E. Mårsell, S. Link, G. Tom, M. Zonno, M. Michiardi, M. Schneider, S. Zhdanovich *et al.*, Sci. Adv. **5**, eaaw5593 (2019).
[21] F. von Oppen, F. Guinea, and E. Mariani, Phys. Rev. B **80**, 075420 (2009).
[22] S. Zhu, J. A. Stroscio, and T. Li, Phys. Rev. Lett. **115**, 245501 (2015).
[23] See Supplemental Material at http://link.aps.org/supplemental/10.1103/PhysRevLett.124.026602 for (i) derive analytic approximate expressions for the synthetic gauge fields, (ii) discuss ways to suppress intervalley scattering, and (iii) present an approximate semiclassical analysis of the current at finite frequency.
[24] H. P. Wei, D. C. Tsui, M. A. Paalanen, and A. M. M. Pruisken, Phys. Rev. Lett. **61**, 1294 (1988).
[25] S. Das Sarma, S. Adam, E. H. Hwang, and E. Rossi, Rev. Mod. Phys. **83**, 407 (2011).
[26] B. I. Halperin, Phys. Rev. B **25**, 2185 (1982).
[27] Y. Imry, *Introduction to Mesoscopic Physics* (Oxford University Press, Oxford, New York, 2002).
[28] R. Prange and S. Girvin, *The Quantum Hall Effect* (Springer, New York, 1990).
[29] S. Datta, *Electronic Transport in Mesoscopic Systems* (Cambridge University Press, Cambridge, England, 1997).
[30] One can also combine the dynamical pseudo-ac voltage V_ω with an external magnetic field B_{ext}. This generates an alternating valley current instead of a charge current, which would not be sensitive to intervalley scattering.
[31] T. Low and F. Guinea, Nano Lett. **10**, 3551 (2010).
[32] P. Ghaemi, S. Gopalakrishnan, and S. Ryu, Phys. Rev. B **87**, 155422 (2013).
[33] A. F. Morpurgo and F. Guinea, Phys. Rev. Lett. **97**, 196804 (2006).
[34] One may imagine adding smoothening backgates parallel to the edges of the narrowing device in order to push the electrons away from the disordered edge of the graphene ribbon, see [23].
[35] S.-P. Lee, D. Nandi, F. Marsiglio, and J. Maciejko, Phys. Rev. B **95**, 174517 (2017).
[36] É. Lantagne-Hurtubise, X.-X. Zhang, and M. Franz, arXiv:1909.01442.
[37] A. Vaezi, N. Abedpour, R. Asgari, A. Cortijo, and M. A. H. Vozmediano, Phys. Rev. B **88**, 125406 (2013).
[38] M. Settnes, N. Leconte, J. E. Barrios-Vargas, A.-P. Jauho, and S. Roche, 2D Mater. **3**, 034005 (2016).
[39] N. Ma, S. Zhang, and D. Liu, Phys. Lett. A **380**, 1884 (2016).
[40] S. Milovanović and F. Peeters, J. Phys. Condens. Matter **29**, 075601 (2017).

[41] M. Settnes, J. H. Garcia, and S. Roche, 2D Mater. **4**, 031006 (2017).
[42] E. Muñoz and R. Soto-Garrido, J. Phys. Condens. Matter **29**, 445302 (2017).
[43] F. Zhai, X. Zhao, K. Chang, and H. Q. Xu, Phys. Rev. B **82**, 115442 (2010).
[44] T. Fujita, M. Jalil, and S. Tan, Appl. Phys. Lett. **97**, 043508 (2010).
[45] Z. Wu, F. Zhai, F. M. Peeters, H. Q. Xu, and K. Chang, Phys. Rev. Lett. **106**, 176802 (2011).
[46] M. Settnes, S. R. Power, M. Brandbyge, and A.-P. Jauho, Phys. Rev. Lett. **117**, 276801 (2016).
[47] T. Stegmann and N. Szpak, 2D Mater. **6**, 015024 (2018).
[48] S. Prabhakar, R. Nepal, R. Melnik, and A. A. Kovalev, Phys. Rev. B **99**, 094111 (2019).
[49] Y. Wu, D. Zhai, C. Pan, B. Cheng, T. Taniguchi, K. Watanabe, N. Sandler, and M. Bockrath, Nano Lett. **18**, 64 (2018).
[50] L. E. Golub, S. A. Tarasenko, M. V. Entin, and L. I. Magarill, Phys. Rev. B **84**, 195408 (2011).
[51] Y. Jiang, T. Low, K. Chang, M. I. Katsnelson, and F. Guinea, Phys. Rev. Lett. **110**, 046601 (2013).
[52] J. Wang, K. Chan, and Z. Lin, Appl. Phys. Lett. **104**, 013105 (2014).
[53] D. I. Pikulin, A. Chen, and M. Franz, Phys. Rev. X **6**, 041021 (2016).
[54] A. G. Grushin, J. W. F. Venderbos, A. Vishwanath, and R. Ilan, Phys. Rev. X **6**, 041046 (2016).
[55] E. V. Gorbar, V. A. Miransky, I. A. Shovkovy, and P. O. Sukhachov, Phys. Rev. B **96**, 125123 (2017).
[56] V. Arjona and M. A. H. Vozmediano, Phys. Rev. B **97**, 201404(R) (2018).
[57] S. Kamboj, P. S. Rana, A. Sirohi, A. Vasdev, M. Mandal, S. Marik, R. P. Singh, T. Das, and G. Sheet, Phys. Rev. B **100**, 115105 (2019).